Journal of Catalysis 265 (2009) 63–71

Contents lists available at ScienceDirect

Journal of Catalysis

journal homepage: www.elsevier.com/locate/jcat

PtNi catalysts prepared via borohydride reduction for hydrogenation of benzene

N.H.H. Abu Bakar [a,b], M.M. Bettahar [a,*], M. Abu Bakar [b], S. Monteverdi [a], J. Ismail [b], M. Alnot [c]

[a] UMR CNRS-UHP 7565, IJB, Faculté des Sciences, Université Henri Poincare, Nancy 1, BP 239, 54506 Vandoeuvre Cedex, France
[b] School of Chemical Sciences, Universiti Sains Malaysia, 11800 Gelugor, P.Pinang, Malaysia
[c] Laboratoire de Physique des Matériaux, UMR 7556, Université Henri Poincare, Nancy 1, BP 239, 54506 Vandoeuvre Cedex, France

ARTICLE INFO

Article history:
Received 13 January 2009
Revised 14 April 2009
Accepted 16 April 2009
Available online 13 May 2009

Keywords:
Pt/Ni bimetallic nanoparticles
Silica support
Impregnation technique
Hydrogenation of benzene

ABSTRACT

Pt/Ni supported on silica catalysts were synthesized via co-impregnation (CI) and step-impregnation (SI) techniques using $NaBH_4$ as the metal ions reducing agent. They were characterized by H_2-TPR and H_2-TPD, XRD, TEM, SEM and EDSX analyses as well as tested for the hydrogenation of benzene. The preparation method employed facilitates the formation of totally reduced pure metal or bimetallic metal particles on the surface and catalytic properties are governed by both the Pt/Ni ratio and mode of preparation. Co-impregnated catalysts exhibit a synergistic effect when a moderate amount of Pt is available: $Pt_{55}Ni_{45}$-CI catalyst was more active than both the pure monometallic catalysts. XRD and SEM equipped with EDSX lead us to believe that alloying occurs in the catalyst. Furthermore, surface segregation of Pt on the alloys as proven by XPS also contributes to this enhanced reactivity. In contrast to co-impregnated catalyst, all the step-impregnated catalysts show low catalytic reactivity when compared to pure Pt.

1. Introduction

The increase in demand for Pt in various industries such as in fuel cell technologies and for petroleum refining has lead to a drastic hike in the price of Pt over the last decade [1]. This has indirectly created an increase in attention towards systems containing bimetallic nanoparticles. The addition of a transition metal to an active metal not only enhances catalytic reactivity but also, in some cases, changes its selectivity. Hence, systems such as Pt/Cu, Pt/In and Pt/Sn supported on H-zeolite have been studied for the conversion of *n*-butane to iso-butene [2], while Pt/Ru supported on carbon has been investigated as a potential polymer electrolyte fuel cell catalysts [3]. Pt/Ni bimetallic nanoparticles supported on ZrO_2 have also been employed for reactions such as the hydrogenation of chloronitrobenzene [4] and cinnamaldehyde [5]. In the hydrogenation of chloronitrobenzene, the $PtNi/ZrO_2$ shows a decrease in hydrogenation activity but an increase in its yield to form chloroaniline [4]. In contrast, better selectivity towards hydrocinnamaldehyde and higher hydrogenation rates with the amount of Ni is observed for the hydrogenation of cinnamaldehyde [5]. Frequently, these superior characteristics are discussed based on the electronic and/or geometric effects that occur when two or more metals are available.

In general, the incorporation of two metals in a system can form alloyed or non-alloyed bimetallic nanoparticles. The alloyed particles may adopt a random alloy or intermetallic structure, while non-alloyed particles may result as cluster in cluster or core–shell structures [6]. The formation of these structures is drastically influenced by the conditions they are synthesized in. Hence, elaborate understanding of factors such as the choice of metal, stabilizer or support employed as well as the method of preparation is essential to design bimetallic nanoparticles suitable for a certain catalytic reaction. As an example, some works have shown that simultaneous reduction of metal ions such as Pt and Pd in stabilizers such as PVP can generate core–shell bimetallic nanoparticles [7], while others have demonstrated that incipient wetness impregnation techniques favour the formation of alloys with a random distribution [8]. This shows the significance of the preparation method employed.

Subsequently, focusing on the preparation techniques of catalysts, the classical methods whereby the metal oxides are reduced via hydrogen reduction are frequently used. Though this technique has the advantage of eliminating the existence of elements that can hinder catalytic activity, it may to some extent result in aggregation or sintering of the metals as well as the support involved. This phenomenon, however, largely depends on the temperature in which hydrogen reduction is conducted [9]. With regard to this, other techniques such as chemical reduction have also been gaining attention. Basically, chemicals such as hydrazine [10], sodium borohydride [11,12] and sodium formate [13] have been used to reduce the metal salts on supports. The ultimate goal is to obtain smaller sized particles that may enhance reaction rates.

As previously mentioned, several factors affect the structures of bimetallic nanoparticles which ultimately influence catalytic

* Corresponding author. Fax: +33 83 68 49 55.
E-mail address: mohammed.bettahar@lcah.uhp-nancy.fr (M.M. Bettahar).

0021-9517/$ - see front matter © 2009 Elsevier Inc. All rights reserved.
doi:10.1016/j.jcat.2009.04.011

activity. Basically it is important to understand that they generally intercorrelate with each other. Hence, it is difficult to obtain the best conditions in which optimum catalytic activity is achieved. Even so, various works have focused on the numerous aspects among which are the choice of metals and support employed. Therefore, in this work our objective is to investigate on how the method of preparation affects the properties of Pt/Ni structures supported on silica. For this purpose, the Pt/Ni–silica was prepared via co-impregnation (CI) and step-impregnation (SI) techniques using $NaBH_4$ as a reducing agent. The characteristics of the samples are investigated in order to gain a better insight on its surface properties and the as formed structures. Further, activities of the catalysts were studied for the hydrogenation of benzene to cyclohexane.

2. Experimental

2.1. Materials

All chemicals were purchased and used without further treatment. Crystalline silica (99.99%) was obtained from Chempure. Hexachloroplatinic acid ($H_2PtCl_6{\cdot}H_2O$) was purchased from Sigma, nickel (II) sulphate ($NiSO_4{\cdot}6H_2O$) from R&M Chemicals and sodium borohydride ($NaBH_4$) from Riedel-de Haen.

2.2. Preparation of catalysts

Stock solutions of $H_2PtCl_6{\cdot}H_2O$ and $NiSO_4{\cdot}6H_2O$ were prepared by dissolving the appropriate amounts of the metal salts in distilled water to obtain a concentration of 0.051 M and 0.084 M, respectively. Various amounts of the Pt and Ni salt solutions were then used to prepare catalysts with different Pt/Ni weight percentages (wt%). The two methods employed are described.

Step-impregnation (SI) technique is a two-step process involving the impregnation and reduction of Ni followed by Pt on the silica support. An amount of silica was weighed and dissolved in 30 ml of distilled water. Argon was bubbled through the colloid at room temperature for a duration of 10 min before the addition of a certain volume of Ni stock solution. The colloid was then homogenized for another 15 min in a similar environment. Subsequently, the liquid phase was evaporated and dried under vacuum conditions. The residue was then ground and immersed in a mixture of distilled water and ethanol. Addition of 0.2 M of fresh cold $NaBH_4$ in inert conditions at 353 K changed the whitish emulsion to a grey colour. The reaction was allowed to continue for a duration of 15 min. The liquid phase was then evaporated and the mixture was dried in vacuum conditions. The Ni catalyst supported on silica was then redispersed in a mixture of distilled water and ethanol. A volume of the previously prepared Pt stock solution was subsequently impregnated and reduced as described for Ni.

Catalysts synthesized via the CI technique were prepared by incorporating various volumes of the Ni and Pt salt solutions in an argon-purged colloidal mixture of silica and distilled water. The mixture was then homogenized for a duration of 15 min before evaporating the liquid phase and drying the residue under vacuum conditions. The silica–metal salt cake was ground and redispersed in a mixture of distilled water and ethanol. The colloid was then purged with argon at 353 K for a duration of 10 min before the addition of 0.2 M fresh cold $NaBH_4$. Finally, the sample was filtered and washed before drying under vacuum conditions.

2.3. Characterization techniques

All characterization analyses were conducted on fresh dried catalysts that were previously reduced with $NaBH_4$.

Surface properties of the catalysts were studied using dynamic flow methods such as H_2-temperature-programmed reduction (H_2-TPR) and H_2-temperature-programmed desorption (H_2-TPD) as well as X-ray photoelectron spectroscopy (XPS). For the H_2-TPR studies as much as 50 mg of the catalysts was weighed and placed in a U-shaped reactor. The reactor was then fixed to a thermocouple and purged with argon to discard excess of oxygen in the setup. Subsequently, diluted H_2 was purged through the reactor from room temperature to 1123 K at a heating rate of 5 K min^{-1}. The amount of H_2 detected is determined using an Agilent G2890A microchromatograph operated at 333 K, at an interval of every 2 min. H_2-TPD experiments were carried out using 50 mg of a catalyst. The catalyst was placed in a reactor and purged with argon followed by activation in pure H_2 for a duration of 15 min at 200 °C. The activated catalysts were then purged with argon before subjecting to a similar temperature programme as the H_2-TPR experiments. XPS analyses on the other hand were conducted using Mg Kα radiations. Scans were carried out to obtain spectra for C 1s, S 2p, O 1s, Ni 2p and Pt 4f.

The morphology of the metal phase in the catalysts was investigated using a transmission electron microscopy (TEM) model Philips CM12 operating at 80 kV. A few drops of the sample suspended in ethanol were placed on the carbon-coated copper grids before analysis. Scanning electron microscopy (SEM) equipped with *x*-mapping was employed to determine the distribution of the Pt, Ni, Si and O components in the catalysts. This was achieved using a Leo Supra 50VP Field Emission Scanning Electron Microscopy (FE-SEM) equipped with an Oxford INCA400 energy dispersive X-ray microanalysis system. The crystallinity of the active phase in the catalysts was determined using X-ray diffraction (XRD) techniques. In this case, fresh catalysts were subjected to a Cu Kα radiation and spectra were recorded in the 2θ range of 10–100°.

2.4. Hydrogenation of benzene

Catalytic activities of the catalysts were investigated via the hydrogenation of benzene. Typically, 50 mg of the catalyst was weighed and placed in a reactor. The catalysts were then purged with argon and were subsequently subjected to a flow of pure H_2 for activation. This was conducted at 200 °C for a duration of 15 min. Following this, catalysts were cooled to room temperature. Hydrogenation of benzene was measured at various temperatures by passing a reaction mixture composed of 10/40/150 ml min^{-1} benzene/hydrogen/helium through the reactor. Reaction products were passed through a 5730A Hewlett–Packard gas chromatography equipped with a flame ionization detector. A molecular sieve column of 2 m in length was used.

3. Results and discussion

3.1. Surface characteristics

3.1.1. H_2-TPR analysis

The active phase in catalysts plays an important role in catalytic reactions. It acts as sites that allow the adsorption of reactant gas molecules and subsequent reaction and conversion to products. This active phase usually comprises transition metals and is most active in its reduced state. In order to gain insight on the state in which these phases exist, H_2-TPR analysis was conducted. H_2-TPR profiles of the Pt_{100} and Ni_{100} catalysts are shown in Fig. 1a. The profile of Pt_{100} does not exhibit any H_2 consumption peaks and hence indicates that the catalyst is in its reduced state.

Contrary to this, the Ni_{100} catalyst exhibits two hydrogen consumption peaks. These peaks are positioned at 677 and 805 K. The peak positioned at approximately 677 K has frequently been

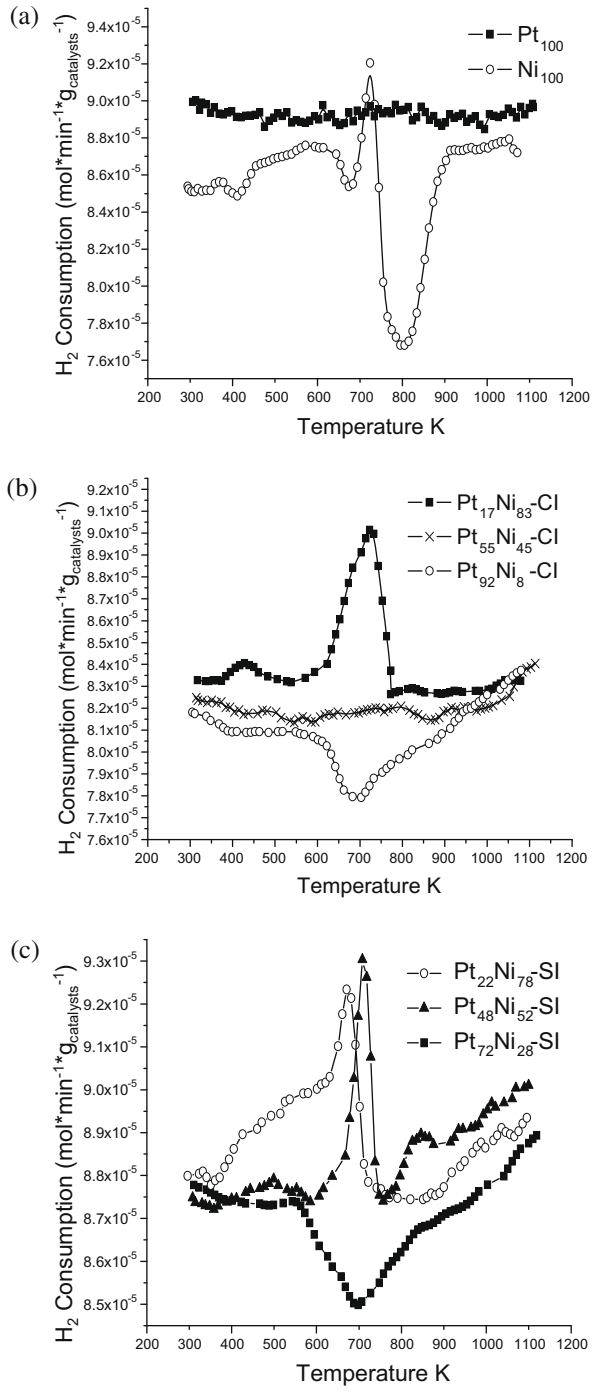

Fig. 1. TPR profiles of (a) Pt_{100} and Ni_{100} catalysts as well as catalysts prepared via (b) CI and (c) SI techniques.

reported to be attributed to the existence of nickel oxides [14,15]. However, the assignment of the peak positioned at 805 K is controversial. Similar to the peak at 677 K, this peak may signify the presence of Ni^{2+} ions in the form of nickel oxides [15]. It is possible that the nickel oxides originate from the re-oxidation of metallic nickel formed during reduction with $NaBH_4$. Oxidation could have occurred during handling or storage of the samples. Hence, the two peaks may be attributed to the occurrence of metal particles with different sizes [15]. The peak at 805 K may be related to larger particles, while the peak arising at 677 K can be attributed to smaller particles. Similar observations were also made by Rynkowski and co-workers [16].

Though this might occur in this work, it is important to consider that the peak at 805 K may also identify the availability of phyllosilicates, which is a type of nickel silicate. This compound occurs via strong interaction between the nickel ions and SiO_2 support [17]. Though SiO_2 is an inert support, it is well established that the impregnation of Ni salts onto SiO_2 leads to strongly and weakly adsorbed Ni^{2+} ions [17,18]. The phyllosilicates are obtained by impregnation of the nickel salt followed by washing and subsequent drying of the catalysts at temperatures below 373 K. The washing stage removes free Ni^{2+} ions which would otherwise form weakly adsorbed Ni^{2+} ions [17]. In this work, the Ni_{100} catalyst was prepared by simple impregnation followed by the drying stage. The catalyst was washed only after reduction with $NaBH_4$. Therefore, the weakly attached Ni^{2+} ions should give rise to large Ni metal particles which may reoxidize upon contact with air, the extent of reoxidation depending on the particle size. Phyllosilicates are not expected to form or exist as a minor species if any.

Subsequently, the impregnation of Ni in the Pt catalysts resulted in the formation of catalysts with slightly different surface properties. The co-impregnated catalysts (Fig. 1b) containing low to moderate amounts of Pt ($Pt_{17}Ni_{83}$-CI and $Pt_{55}Ni_{45}$-CI) exhibited no hydrogen consumption in the temperature range studied. Similar to the pure Pt catalysts, this signifies that total metal reduction occurred during the reduction stage with $NaBH_4$. In comparison, the catalysts with high Pt content demonstrated a consumption of hydrogen at approximately 679 K. Total H_2 consumption of the $Pt_{92}Ni_8$-CI catalyst is 1.33×10^{-3} mol $g^{-1}_{(metal)}$. This corresponds to 21.7% of the total mol metal content existing as oxides. In accordance with the peak position, we attribute this H_2 consumption as due to the occurrence of nickel oxide.

The catalysts prepared via step-impregnation technique also showed similar hydrogen consumption trends with those prepared via co-impregnation technique. This is shown in Fig. 1c. Both the $Pt_{22}Ni_{78}$-SI and $Pt_{48}Ni_{52}$-SI catalysts showed no hydrogen consumption, while catalysts with high Pt content ($Pt_{72}Ni_{28}$-SI) demonstrated a consumption of 4.50×10^{-3} mol $g^{-1}_{(metal)}$ at 689 K. This is similar to the hydrogen consumption peak in the pure Ni catalyst and amounts to 52.9% of the total mol metal content.

The occurrence of metal oxides or more specifically nickel oxides in catalysts with high Pt content, regardless of the preparation method employed, can only be explained as due to the occurrence of Pt and Ni existing as separate entities. The profiles clearly demonstrate that in these catalysts, Pt does not catalyze total reduction of the nickel oxides. This phenomenon is surprising and is yet to be fully understood.

Another interesting feature observed for the Ni_{100} catalyst as well as for both the co and step-impregnated catalysts with more than 50% Ni content, is that a maximum H_2 production is seen at approximately 630–740 K. Profiles of Ni_{100}, $Pt_{17}Ni_{83}$-CI as well as $Pt_{22}Ni_{78}$-SI and $Pt_{48}Ni_{52}$-SI catalysts indicate that maximum H_2 desorbed at temperatures of 735 K (1.73×10^{-3} mol $g^{-1}_{(metal)}$), 727 K (3.63×10^{-3} mol $g^{-1}_{(metal)}$), 679 K (9.10×10^{-4} mol $g^{-1}_{(metal)}$) and 720 K (2.10×10^{-3} mol $g^{-1}_{(metal)}$) for the four catalysts, respectively. This shows that similar H_2 adsorption sites exist in the catalysts. Some hydrogen desorption is also seen at higher temperatures. The adsorption of hydrogen may have originated from two possibilities. First, adsorption of H_2 may have occurred during the reduction stage. Hydrogen gas that is produced during the reduction of metal ions with $NaBH_4$ may have adsorbed onto certain phases of the metal structure. Second, the TPR analysis was preformed in a H_2 atmosphere. Hence, it is possible that H_2 gas adsorbed at lower temperatures is desorbed at higher temperatures. Similar behaviour has been observed for Pd-supported SiO_2 catalysts [19]. In the case of Pd, the hydrogenation reactions form a hydride that acts as a reversible storage medium for active hydrogen [20].

3.1.2. H_2-TPD Analysis

The H_2-TPD profiles of the Pt_{100} and Ni_{100} catalysts are exhibited in Fig. 2a. Both catalysts show very different characteristics. The H_2-TPD profile of Ni_{100} indicates two main peaks positioned at 621 K and 741 K. These peaks coincide roughly with the H_2-TPR profiles. The peak at 621 K is attributed to H_2 strongly adsorbed onto the Ni surface while the desorption band occurring at 741 K can be explained as due to hydrogen retained at the interphase of the metal support [21]. As much as 2.34×10^{-3} mol $g^{-1}_{(metal)}$ hydrogen is desorbed from this catalyst. In contrast, the H_2-TPD analysis of Pt_{100} shows an almost flat profile. It is interesting to note that very little desorption occurred for this catalyst. This occurrence can be explained as due to the hydrogen weakly adsorbed onto the Pt surface when compared to Ni which is more strongly adsorbed to hydrogen. The difference in adsorption characteristics of Pt and Ni can be explained based on their positions in the periodic table. Atoms at the top of the periodic table such as Ni generally have stronger chemisorption characteristics compared to atoms positioned further down such as Pt. This is due to the increase in the occupancy of the d bands in the Pt atoms. The lower strength of adsorption for Pt_{100} may have caused the hydrogen adsorbed during activation to desorb during the purging treatment following the activation. Hence, this explains the lack of hydrogen desorption during the H_2-TPD analysis for catalysts with high Pt content.

Subsequently, H_2-TPD profiles of the bimetallic catalysts were investigated. It is observed that CI catalysts exhibit two types of catalysts. The profiles are shown in Fig. 2b. The first type is of $Pt_{17}Ni_{83}$-CI. This catalyst shows characteristics similar to those of Ni_{100}. Two peaks positioned at 613 K and 732 K are observed. These peaks are shifted to lower temperatures when compared to those of Ni_{100}. The shifts can be explained as due to the addition of platinum in the samples. Following this, a high amount of H_2 (5.02×10^{-3} mol $g^{-1}_{(metal)}$) was desorbed from the catalyst when compared to that desorbed from Ni_{100}. We attribute this to the incorporation of H_2 during the reduction stage as well as during the activation stage. This correlates well with the H_2-TPR profiles. The second type of catalysts observed is for the samples $Pt_{55}Ni_{45}$-CI and $Pt_{91}Ni_8$-CI. Both the catalysts can be described as similar to the pure Pt type. Very little desorption is observed, hence it is possible to summarize that these bimetallic catalysts imitate the characteristics of pure Pt.

The SI catalysts as presented in Fig. 2c also show two types of catalysts. However, in contrast to the types observed in the CI technique, a separate type of catalyst is also observed. The first type of catalysts includes $Pt_{22}Ni_{78}$-SI and $Pt_{48}Ni_{52}$-SI. These catalysts are comparable to Ni_{100} and $Pt_{17}Ni_{83}$-CI. It is observed that the desorption peaks for $Pt_{22}Ni_{78}$-SI and $Pt_{48}Ni_{52}$-SI are also shifted to lower temperatures in the range of 620–625 K and 710–715 K. On the other hand, the second type of catalyst is solely $Pt_{72}Ni_{28}$-SI. This type of catalysts was not observed in the samples prepared via the previous method. Though $Pt_{72}Ni_{28}$-SI exhibits two peaks, both are positioned at temperatures much lower than those of the first type. Deconvolution of the TPD profiles indicates that the peaks arise at 623 K and 667 K. These peaks are characteristic of hydrogen strongly attached to the Ni particle or hydrogen which exists at the metal support interphase [21].

Based on the surface properties investigated, it is found that two main types of catalysts occur: catalysts that are characteristic of Ni_{100} and catalysts that are characteristic of Pt_{100}. Only $Pt_{72}Ni_{28}$-SI shows properties unlike the previous two types.

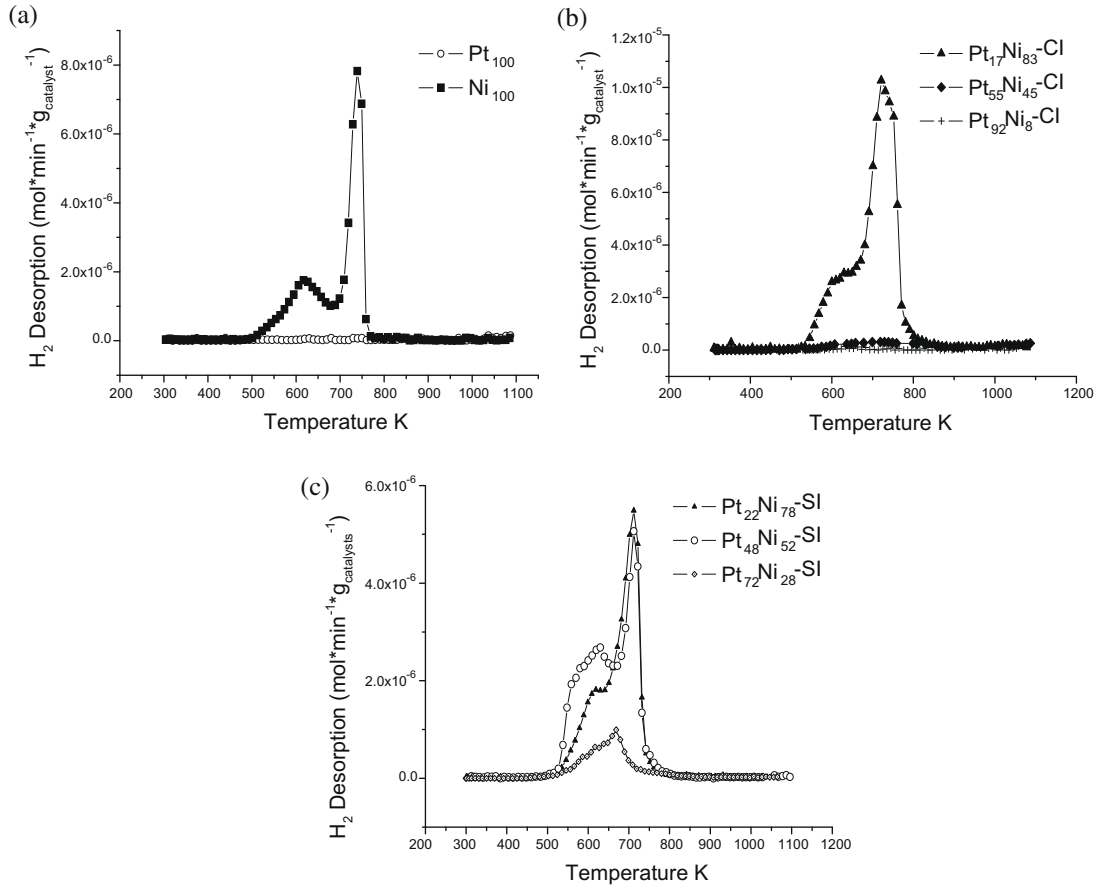

Fig. 2. TPD profiles of (a) Pt_{100} and Ni_{100} catalysts as well as Pt/Ni catalysts supported on silica prepared via (b) CI and (c) SI techniques.

3.2. TEM analysis

The morphology of the catalysts was studied using TEM analysis. Images of the Pt_{100}, Ni_{100} and typical images of the bimetallic catalysts are exhibited in Fig. 3. As can be seen, all samples demonstrate the formation of fractals. Similar morphologies have been observed elsewhere [22,23]. These fractals occur due to the agglomeration of smaller metal particles. The images demonstrate that the particles in all samples are spherical in shape. However, an interesting feature in the Ni_{100} and $Pt_{48}Ni_{52}$-SI catalysts is that the spherical particles are surrounded by a thin shell. This shell has been described to be a layer of oxide surrounding the metal core [24,25]. Such a phenomenon was not observed in the Pt_{100} and the bimetallic $Pt_{55}Ni_{45}$-CI catalysts. Hence, this shows that oxidation of Ni_{100} and $Pt_{48}Ni_{52}$-SI occurred during the preparation or storage stage. Even so the degree of oxidation in both samples varies. As was observed in the H_2-TPR studies, large hydrogen consumption is observed for Ni_{100}, hence indicating that extensive oxidation occurred. In contrast, no hydrogen consumption was seen in the TPR profiles of $Pt_{48}Ni_{52}$-SI catalyst. Therefore, it is possible that little oxidation occurred in this sample. Such a phenomenon may be explainable as due to the existence of Pt that changes the adsorption properties of the synthesized catalyst.

Following this, average sizes of the particles are obtained and reported in Table 1. A comparison of the average particle sizes of Pt_{100} and Ni_{100} shows that the Ni particles are approximately five times larger than the Pt particles. This may be attributed to the magnetic nature of the Ni catalysts, which promotes particle agglomeration. Upon alloying Pt and Ni, it is seen that the average size of the particles decreased significantly with the increase in Pt

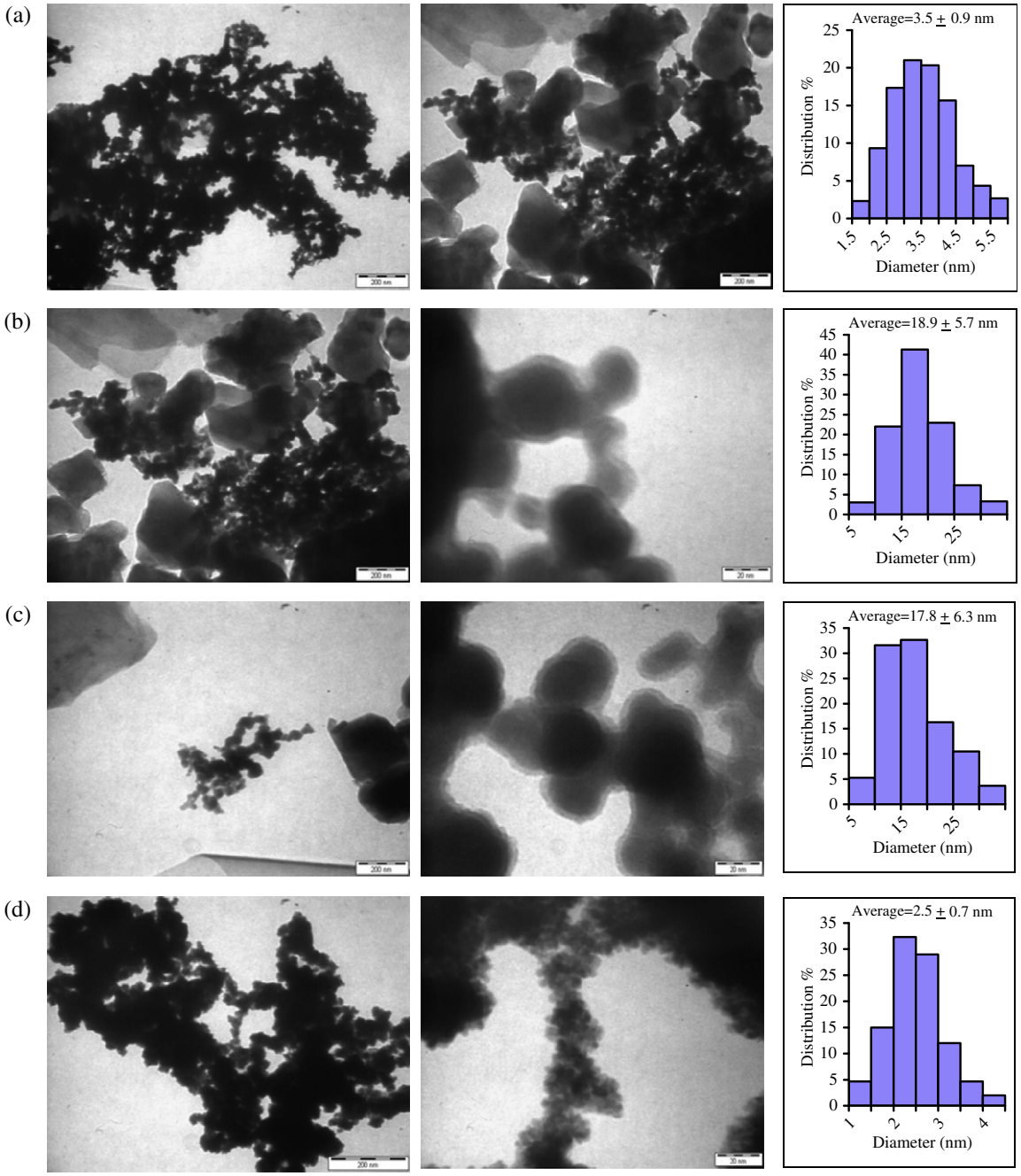

Fig. 3. TEM micrographs of (a) Pt_{100}, (b) Ni_{100}, (c) $Pt_{48}Ni_{52}$-SI and (d) $Pt_{55}Ni_{45}$-CI and their corresponding histograms on size distribution.

Table 1
Physico-chemical characteristics of supported silica catalysts.

Catalysts	Impregnation method	Total metal loading	Metal compositions		Atomic percentages		Average particle size (nm)	Dispersion (%)
			Pt	Ni	Pt	Ni		
Pt_{100}	–	2.63	2.63	–	100	–	3.5 ± 0.9	41.3
$Pt_{17}Ni_{83}$	CI	4.40	0.77	3.63	6.0	94.0	7.3 ± 5.0	11.0
$Pt_{55}Ni_{45}$	CI	2.35	1.29	1.06	26.8	73.2	2.5 ± 0.6	54.0
$Pt_{92}Ni_{8}$	CI	2.25	2.06	0.19	76.5	23.5	2.4 ± 0.6	54.1
$Pt_{22}Ni_{78}$	SI	3.58	0.77	2.81	7.6	92.4	9.7 ± 5.8	10.9
$Pt_{48}Ni_{52}$	SI	3.36	1.62	1.74	21.9	78.1	17.9 ± 6.3	8.9
$Pt_{72}Ni_{28}$	SI	2.89	2.07	0.82	43.1	56.9	2.3 ± 0.5	58.0
Ni_{100}	–	4.21	–	4.21	–	100	18.8 ± 5.7	7.3

content when compared to that of the pure Ni catalyst. A comparison of the $Pt_{17}Ni_{83}$-CI and $Pt_{22}Ni_{78}$-SI catalysts show that the average sizes of the particles are 7.3 ± 5.0 and 9.7 ± 5.8 nm, respectively. Similarly, the $Pt_{55}Ni_{45}$-CI and $Pt_{48}Ni_{52}$-SI catalysts give average particle sizes of 2.5 ± 0.6 and 17.9 ± 6.3 nm, respectively. The difference in the average sizes of the bimetallic nanoparticles, prepared via different techniques but with similar Pt/Ni compositions, may indirectly affect the reactivity of the catalysts due to the variation in surface area available for reaction.

The dispersion of the metal phase in the catalysts was calculated based on the size distribution of the nanoparticles using the mathematical method described by Borodzinski and Bonarowska [26]. This technique was also applied by Yang et al. who studied the synthesis of Pt/Ni nanoparticles for catalytic application [27]. In general, only the bimetallic $Pt_{55}Ni_{45}$-CI, $Pt_{92}Ni_{8}$-CI and $Pt_{72}Ni_{28}$-SI catalysts showed a high percentage of dispersion. Dispersion of the active phase is 54.0%, 54.1% and 58.0%, respectively. This is comparable to the dispersion percentage of Pt_{100} which is 41.3%. Other bimetallic catalysts on the other hand showed low dispersion values similar to that shown by Ni_{100}, which is 7.3%.

3.3. Catalytic activity

A control sample of silica impregnated with $NaBH_4$ was activated at 473 K in a flow of pure H_2. The sample that was exposed to a reaction stream containing benzene showed that no cyclohexane was detected, indicating no conversion. Therefore the support and reducing agent used are inactive towards gas phase hydrogenation of benzene.

Reaction rates of the Pt_{100} and Ni_{100} catalysts as well as the bimetallic catalysts prepared via CI and SI techniques are depicted

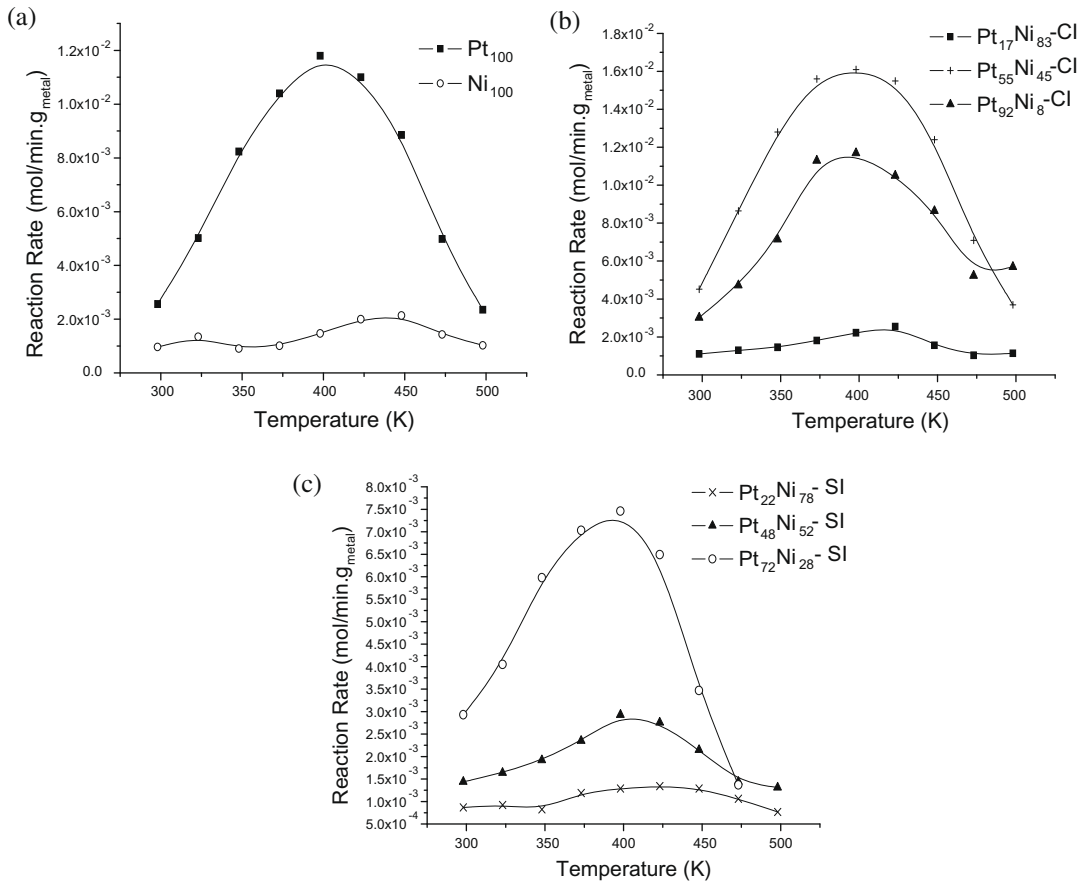

Fig. 4. Reaction rates of hydrogenation of benzene for (a) Pt_{100} and Ni_{100} as well as Pt/Ni catalysts prepared via (b) CI and (c) SI techniques. All reactions were carried out in a reaction flow of C_6H_6:H_2:He 10:40:150 ml/min at atmospheric pressure.

in Fig. 4a–c. It was found that the reaction rate is dependant on the Pt/Ni composition, temperature of reaction and preparation method. The Ni_{100} catalyst shows a nearly constant reaction rate in the temperature range of 298–347 K. The rate of reaction then increases until it reaches a maximum of about 2.14×10^{-3} mol min^{-1} g_{met}^{-1} at 431 K. In contrast, pure Pt is active even at low temperatures. The reaction rate at 298 K is 2.56×10^{-3} mol min^{-1} g_{met}^{-1} and a maximum reaction rate of 1.18×10^{-2} mol min^{-1} g_{met}^{-1} is obtained when temperature reaches 400 K. This is approximately 5-fold the conversion of the Ni_{100} sample.

Generally, the formation of bimetallic Pt/Ni catalysts improves the reaction rate of benzene hydrogenation when compared to that of Ni_{100}. However, for samples prepared via SI technique, the reaction rate of the catalysts with 22% of Pt ($Pt_{22}Ni_{78}$-SI) is lower than that of Ni_{100}. Only upon addition of the Pt content to 52% and 72% is there an improvement in the catalytic activity of the samples. Reaction rates of the catalysts increased to 2.85×10^{-3} and 7.30×10^{-3} mol min^{-1} g_{met}^{-1}, respectively. Here, it can be seen that for this preparation technique, reaction rates increased with the amount of Pt added to the catalysts.

Interestingly, when the bimetallic catalysts were prepared via CI technique, better reaction rates were seen when compared to those prepared via the SI technique. Comparison of the $Pt_{17}Ni_{83}$-CI catalysts with the $Pt_{22}Ni_{78}$-SI catalysts shows that the sample prepared via CI is enhanced by approximately 2-fold. The reaction rate of the $Pt_{17}Ni_{83}$-CI catalyst is 2.55×10^{-3} mol min^{-1} g_{met}^{-1}. Addition of Pt to 55% ($Pt_{55}Ni_{45}$-CI) in the catalysts resulted in a drastic increase in reaction rate. Maximum rate reached 1.59×10^{-2} mol min^{-1} g_{met}^{-1} at 397 K. This is approximately five times higher than the catalyst with similar Pt/Ni compositions prepared via SI and 25% more than the reaction rate obtained for Pt_{100}. Even so, upon further increase in the Pt content to 92% ($Pt_{92}Ni_8$-CI), it was observed that the conversion of benzene to cyclohexane decreased to similar reaction rates as that of Pt_{100}.

Further comparison of the Pt atomic percentage in the $Pt_{55}Ni_{45}$-CI catalysts shows that only 26.8 at% of Pt is available when compared to the Pt_{100} catalysts. The striking enhancement in the hydrogenation of benzene to cyclohexane can be attributed to the synergistic effect which occurs when Pt and Ni are in proximity to each other. The smaller average Pt/Ni particle size in $Pt_{55}Ni_{45}$-CI (2.5 ± 0.6 nm) may also play a role in preparing a larger surface area available for reaction to occur, hence leading to the superior reactivity observed. However, this is not always the case considering that the $Pt_{92}Ni_8$-CI (76.5 at%) and $Pt_{72}Ni_{28}$-SI (43.1 at%) catalysts also have similar average particle size but lower reactivity values. Generally speaking, factors such as the method of preparation or Pt/Ni ratio influence the particles size and shape of metal-based catalysts. The similarity of the particle sizes is only a coincidence. The fractal morphologies evidenced by TEM are roughly different and this may explain the different activities observed. Fractals can be described by their fractal dimensions (D_F), which are characteristic of the porosity of the catalyst. Variations in this porosity can influence the diffusion and reaction phenomenon. Hence, the reactivity of the catalysts depends on the fractals formed. It has been shown that the energy of activation is dependant on the D_F of the catalyst [28]. Though previous works have discussed the reactivity of catalysts in terms of the D_F of metal-supported catalysts whereby the support exhibits fractal morphologies [29,30], we emphasize that in this work the very low surface area of the support and mild reduction conditions may not have played a role in changing the characteristics of the support. In contrast, the fractal nature of the active phase may be responsible for the variation in reactivity observed. A separate study is required to further understand how the D_F of the active phase influences the catalytic reactivity.

In general, at high Ni metal loadings the catalytic activity of the catalysts imitates that of Ni_{100} due to the dominance of the Ni content. However, as the Ni content is reduced, a synergistic effect of the metals involved results in the enhancement in catalytic activity. This effect is then less observed when Pt is more dominant in the catalysts. In this case, the Pt/Ni catalyst imitates the nature of the Pt_{100} catalysts resulting in similar reaction rates.

3.4. Characteristics of $Pt_{55}Ni_{45}$-CI catalyst

To understand the factors that may have caused the enhanced catalytic activity of the $Pt_{55}Ni_{45}$-CI catalyst, various analyses were

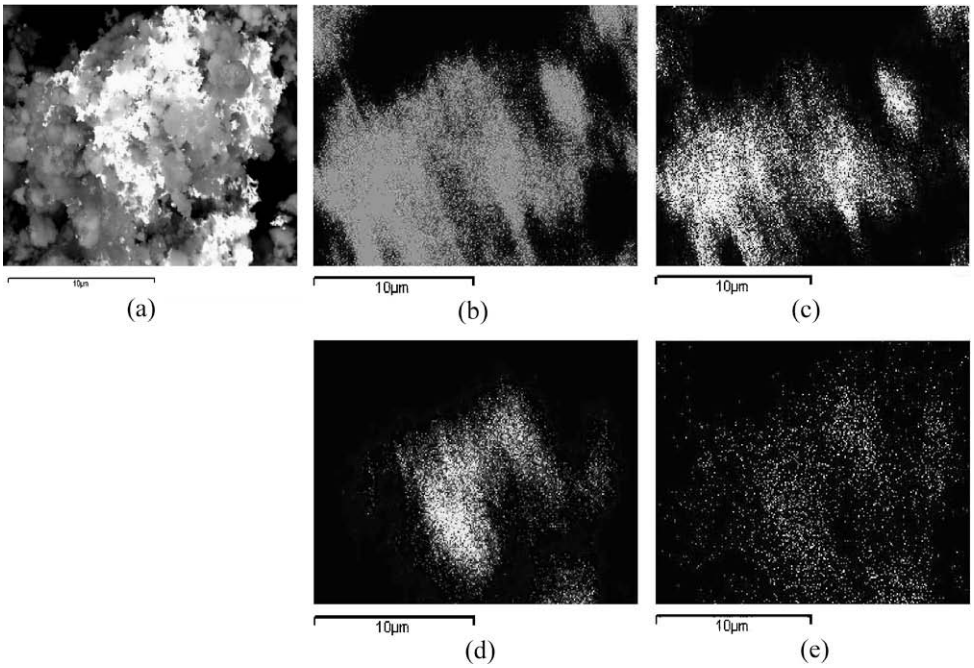

Fig. 5. (a) SEM micrographs of $Pt_{55}Ni_{45}$-CI and corresponding distributions of (b) Si, (c) O, (d) Pt and (e) Ni.

carried out. SEM analysis with mapping of the $Pt_{55}Ni_{45}$-CI catalyst was conducted to investigate the distribution of the bimetallic nanoparticles on the silica. The darker area in the image of Fig. 5a is of the silica support. The distribution of Si is consistent with that of O. The brighter area in the image can be attributed to the metal phase. This correlates well with the distribution of Pt and Ni. Considering that similar distribution is observed for both the metals, it is highly likely that alloying of the metals occurred in the catalyst.

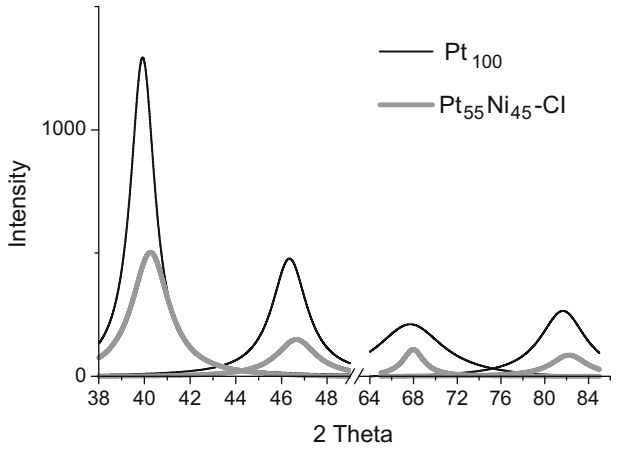

Fig. 6. XRD diffractograms of Pt_{100} and $Pt_{55}Ni_{45}$-CI catalysts prepared via co-impregnation. Diffractograms are obtained after subtraction of the silica peaks.

To confirm the mapping analysis, XRD diffractograms of the fresh Pt_{100}, Ni_{100} and $Pt_{55}Ni_{45}$-CI catalysts were studied. However, subtraction of the silica diffractograms from the XRD diffractograms of the catalysts and further deconvolutions were necessary as the peaks of crystalline silica were superimposed with those of Pt. The XRD patterns are depicted in Fig. 6. As can be seen, Pt_{100} shows the existence of peaks positioned at 2θ values of 39.91, 46.31, 67.76 and 81.71. These peaks are indicative of the (111), (200), (220) and (311) planes of the *fcc* crystalline structured Pt particles. Therefore, Pt exists in its reduced state in the fresh catalyst. For the Ni_{100} supported on silica catalyst, no peaks indicating the existence of Ni are observed. Thus, considering the large-sized particles obtained via size distribution analysis, this shows that the Ni exists in an amorphous phase. Consequently, upon reduction of Ni ions in the presence of Pt, we found that for $Pt_{55}Ni_{45}$-CI, only Pt peaks were observed, these peaks are shifted to higher 2θ values and are positioned at 40.23, 46.69, 67.98 and 82.26. This shift in the 2θ values is attributed to the alloying of the metals involved. Thus in this work, Ni is incorporated into the Pt structure. In addition, the average size of the nanoparticles formed based on the XRD analysis can be calculated using the Scherrer equation. Values of 3.9 and 4.2 nm were obtained for the samples Pt_{100} and $Pt_{55}Ni_{45}$-CI, respectively. These values differ from those obtained via TEM analysis and can be explained as due to the particle–particle interaction that may occur when particles are positioned close to each other.

To further investigate the nature of the catalyst, XPS measurements of Pt_{100} and Ni_{100} were investigated and compared with the profile of $Pt_{55}Ni_{45}$-CI catalyst. The profile of the Pt 4f region in Fig. 7a exhibits doublet peaks at 71.4 and 74.8 eV. These peaks

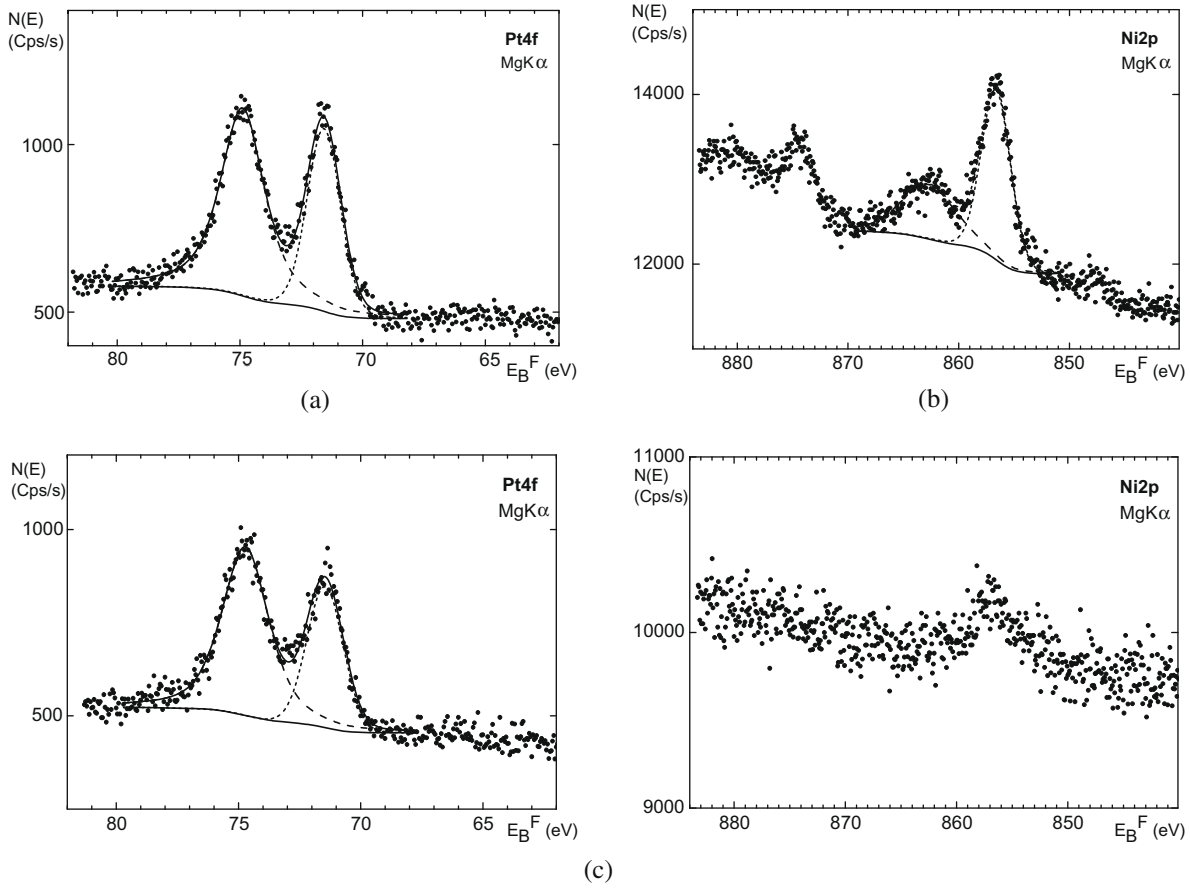

Fig. 7. XPS profiles of (a) Pt_{100}, (b) Ni_{100} and (c) $Pt_{55}Ni_{45}$-CI.

correspond to Pt $4f_{7/2}$ and Pt $4f_{5/2}$ signals of metallic Pt. This correlates well with the TPR profiles of Pt_{100} as well as with the XRD diffractograms.

Subsequently, analysis of the states in which the nickel exists in the Ni_{100} catalyst was studied. Two prominent peaks at 856.9 and 862.4 eV are obtained in the Ni $2p_{3/2}$ spectrum. The peak positioned at 862.4 eV is known as the satellite peak that appears as a result of multi-electron excitation [31,32]. The occurrence of the peak at 856.9 eV on the other hand is ambiguous. In general, various works have reported that this peak can be attributed to the occurrence of Ni hydroxides in the samples and that deconvolution of this peak may give rise to several other peaks that indicate the occurrence of NiO as well as metallic Ni depending on the broadness of the peak [31]. However, it has been shown that for Ni-supported SiO_2 systems this peak can be attributed to the occurrence of nickel silicate ($NiSiO_3$). This indicates that the formation of phyllosilicates occurs to some extent. Considering the broadness of the peak which arises starting from 852.9 to 859.6 eV, it is also possible that the NiO or Ni_2O_3 peak overlaps with this peak. Both oxides usually exhibit a maximum at 854.0–854.9 eV and 856.0 eV, respectively [33,34]. This corresponds to the H_2-TPR profiles discussed previously.

Investigation of the bimetallic nanoparticles reduced simultaneously reveals that signals indicating the presence of Pt in the Pt 4f spectra are seen. These signals are positioned at BE values of 71.3 and 74.6 eV. The positions of the peaks similar to those of the Pt_{100} catalyst designate that metallic Pt exists in the samples. However, comparison of the BE shows a difference of 0.1 and 0.2 eV, respectively. This shift to lower binding energies is due to the formation of metallic bonds or alloying that occurs at low temperatures [35]. Interestingly, no peaks are seen in the Ni 2p spectra. This phenomenon can be explainable as due to surface segregation of the Pt metal phase on the surface of the bimetallic nanoparticles.

To summarize, based on the properties of $Pt_{55}Ni_{45}$-CI catalyst, it is obvious that this catalyst exhibits unique properties superior to those of Pt_{100} and Ni_{100}. Its small particle size and high distribution, combined with the surface segregation of Pt on the bimetallic nanoparticles and alloying of the metal phases involved, all contribute to the enhanced catalytic activity of benzene hydrogenation.

4. Conclusions

Our findings show that surface and catalytic properties are governed by both the Pt/Ni ratio and the method of preparation. The preparation method employed can facilitate the formation of totally reduced pure metal or bimetallic metal particles. This reduced state is maintained after handling and storage in air for Pt_{100} as well as moderate and low Pt content bimetallic catalysts. For Ni_{100} and low Ni content bimetallic metal particles, oxidation occurred. Co-impregnated catalysts exhibit enhanced reactivity when compared to step-impregnated catalysts. An activity superior to that of Pt_{100} is seen when a moderate amount of Pt is incorporated via co-impregnation technique ($Pt_{55}Ni_{45}$-CI catalyst). This improved activity is striking considering that it only contains 26.8 at% of Pt when compared to the pure Pt catalyst. Our further investigations on the characteristics of $Pt_{55}Ni_{45}$-CI using SEM with x-mapping analysis as well as XRD lead us to believe that alloying occurs in the catalyst. Furthermore, the surface segregation of Pt on the alloys as proven by XPS results also contributes to this enhanced reactivity.

In conclusion, our results correlate well with each other showing that the co-impregnation technique used to prepare the catalysts is superior to the step-impregnation technique. In addition, the novelty lies in the fact that a simple non-classical method can be employed to prepare alloyed catalysts which can be activated at low temperatures for short durations and still exhibit enhanced reactivity when compared to the pure Pt catalyst.

Acknowledgments

The authors would like to acknowledge the financial support from Communauté Urbaine du Grand Nancy, University Sains Malaysia, Université Henri Poincarée, the French and Malaysian governments for the Co-tutelle and ASTS scholarship for N.H.H. Abu Bakar.

References

[1] J. Chen, B. Lim, E.P. Lee, Y. Xia, Nano Today 4 (2009) 81.
[2] S. Scriè, G. Burgio, C. Crisafulli, S. Minico, J. Mol. Catal. A: Chem. 260 (2006) 109.
[3] J. Kaiser, L. Colmenares, Z. Jusys, R. Mortel, H. Bonnemann, G. Kohl, H. Modrow, J. Hormes, R.J. Behm, Fuel Cells 06 (2006) 190.
[4] X.-X. Han, R.-X. Zhou, G.-H. Lai, X.-M. Zheng, Reac. Kinet. Catal. Lett. 83 (2004) 55.
[5] X. Han, R. Zhou, B. Yue, X. Zheng, Catal. Lett. 109 (2006) 157.
[6] N. Toshima, T. Yonezawa, New J. Chem. 22 (1998) 1179.
[7] N. Toshima, M. Harada, T. Yonezawa, K. Kushibashi, K. Asakurat, J. Phys. Chem. 95 (1991) 7448.
[8] W. Shen, F.E. Huggins, N. Shah, G. Jacobs, Y. Wang, X. Shi, G.P. Huffman, Appl. Catal. A: Gen. 351 (2008) 102.
[9] J. Mikulova, J. Barbier Jr., S. Rossignol, D. Mesnard, D. Duprez, C. Kappenstein, J. Catal. 251 (2007) 172.
[10] M. Zielinski, R. Wojcieszak, S. Monteverdi, M. Mercy, M.M. Bettahar, Int. J. Hyd. Energy 32 (2007) 1024.
[11] J. Zeng, J.Y. Lee, Mater. Chem. Phys. 104 (2007) 336.
[12] C. Kim, H.-H. Kwon, I.K. Song, Y.-E. Sung, W.S. Chung, H.-I. Lee, J. Power Sources 171 (2007) 404.
[13] L. Xiong, A.M. Kannan, A. Manthiram, Electrochem. Commun. 4 (2002) 898.
[14] K. Nagaoka, K. Sato, H. Nishiguchi, Y. Takita, Appl. Catal. A: Gen. 327 (2007) 139.
[15] A. Saadi, R. Merabti, Z. Rassoul, M.M. Bettahar, J. Mol. Catal. A: Chem. 253 (2006) 79.
[16] J. Rynkowski, D. Rajski, I. Szyszka, J.R. Grzechowiak, Catal. Today 90 (2004) 159.
[17] M. Che, Z.X. Cheng, C. Louis, J. Am. Chem. Soc. 117 (1995) 2008.
[18] C. Louis, Z.X. Cheng, M. Che, J. Phys. Chem. 97 (1993) 5703.
[19] P.S.S. Prasad, N. Lingaiah, P.K. Rao, F.J. Berry, L.E. Smart, Catal. Lett. 35 (1995) 345.
[20] R. Wojcieszak, M. Zielinski, S. Monteverdi, M.M. Bettahar, J. Coll. Inter. Sci. 299 (2006) 238.
[21] S. Chettibi, R. Wojcieszak, E.H. Boudjennad, J. Belloni, M.M. Bettahar, N. Keghouche, Catal. Today 113 (2006) 157.
[22] L. Zhang, A. Manthiram, Appl. Phys. Lett. 70 (1997) 2469.
[23] W. Zhang, X. Quan, J. Wang, Z. Zhang, S. Chen, Chemosphere 65 (2006) 58.
[24] Q.A. Pankhurst, A.Y. Martinez, L.F. Barquin, Phys. Rev. B 69 (2004) 212401.
[25] J.T. Nurmi, P.G. Tratnyek, V. Sarathy, D.R. Baer, J.E. Amonette, K. Pecher, C. Wang, J.C. Linehan, D.W. Matson, R.L. Penn, M.D. Driessen, Environ. Sci. Technol. 39 (2005) 1221.
[26] A. Borodzinski, M. Bonarowska, Langmuir 13 (1997) 5613.
[27] H. Yang, W. Vogel, C. Lamy, N. Alonso-Vante, J. Phys. Chem. B 108 (2004) 11024.
[28] A.I. Trypolskyi, T.M. Gurnyk, P.E. Strizhak, Chem. Phys. Lett. 460 (2008) 492.
[29] M. Tatlier, L.K. Minsker, Catal. Comm. 6 (2005) 731.
[30] M.O. Coppens, G.F. Froment, Chem. Eng. Sci. 51 (1996) 2283.
[31] T.C. Deivaraj, W. Chen, J.Y. Lee, J. Mater. Chem. 13 (2003) 2555.
[32] K.-W. Park, J.-H. Choi, B.K. Kwoon, S.-A. Lee, Y.-E. Sung, H.Y. Ha, S.-A. Hong, H. Kim, A. Wieckowski, J. Phys. Chem. B 106 (2002) 1869.
[33] Y. Matsumura, K. Tanaka, N. Tode, T. Yazawa, M. Haruta, J. Mol. Catal. A: Chem. 152 (2000) 157.
[34] D. Jo, J.S. Lee, K.H. Lee, J.Mol. Catal. A: Chem. 222 (2004) 199.
[35] K.-W. Park, J.-H. Choi, Y.-E. Sung, J. Phys. Chem. B 107 (2003) 5851.